

Charge redistribution in electrochemically-actuated mechanical sensors

F. Amiot ^{a,*} F. Kanoufi ^b F. Hild ^c J.P. Roger ^d

^a*Institut FEMTO-ST, CNRS-UMR 6174 / UFC / ENSMM / UTBM,
24, chemin de l'Épitaphe, F-25030 Besançon, France.*

^b*PECSA, CNRS-UMR 7195 / ESPCI,
10 rue Vauquelin, F-75231 Paris Cedex 05, France.*

^c*LMT Cachan, ENS de Cachan / CNRS-UMR 8535 / Univ. Paris 6 / PRES
UniverSud Paris*

61 avenue du Président Wilson, F-94235 Cachan Cedex, France.

^d*Institut Langevin / ESPCI ParisTech / CNRS UMR 7587,
Laboratoire d'Optique Physique,
10 rue Vauquelin, F-75231 Paris Cedex 05, France.*

Abstract

Many proofs of concept studies have established the mechanical sensitivity of functionalized microcantilevers to a large spectrum of target molecules. However, moving to real-life applications also requires the monitored mechanical effect to be highly specific. Moving towards more specificity in cantilever-based sensing, monitoring the mechanical response of electrochemically actuated microcantilevers is then thought to provide a fast, reliable and complementary experimental information to the long-time cantilever bending measurement for the detection of target molecules. Full-field measurements are therefore used to investigate the way the electro-elastic coupling is altered when a microcantilever undergoes decane-thiol adsorption. The proposed technique reveals that the latter results in a charge density redistribution along the cantilever in addition to the local surface passivation. Focusing on the cantilever tip displacement under electrochemical actuation, this redistribution partially compensates the electro-elastic coupling alteration due to the surface passivation, therefore possibly yielding an ambiguous detection result. This effect should be taken into account for the optimal design of specific electrochemically actuated mechanical sensors.

Key words: Cantilever-based sensors, Full-field measurements, Identification problem, Microscopy of surfaces, Surface strains

* Corresponding author, fabien.amiot@femto-st.fr

Email addresses: fabien.amiot@femto-st.fr (F. Amiot),
frederic.kanoufi@espci.fr (F. Kanoufi), hild@lmt.ens-cachan.fr (F. Hild),
jean-paul.roger@espci.fr (J.P. Roger).

1 Introduction

Decreasing the size of mechanical objects induces an increase of their surface / volume ratio, and thus their ability to interact with their environment. That is the main reason for the development of MEMS-based bio-chemical sensors. One of the object surfaces is functionalized to allow for chemical recognition of a target molecule. When bonding occurs (regardless of its type), two types of detection schemes are possible [1], namely, one monitors the resonance frequency shift induced by mass changes, or one measures the quasi-static induced bending arising from surface free-strains.

The measurement of the resonance frequency shift is used to detect mass variations [2,4,3] and then to resolve small amounts of biological material [5]. This resonant frequency shift appears in conjunction with a surface free-strain, which is preferably measured in liquids to detect DNA hybridization [6] for instance. In low viscosity media, this quasi-static bending measurement is carried out together with the resonance frequency shift to provide a more robust detection procedure [7]. On the one hand, the detection specificity may be improved by tailoring the used coatings. On the other hand, a fast and user-controlled query mechanism of the cantilever mechanical state is highly desirable to move towards real-life applications.

The coupling between electrochemical and mechanical effects involves small elastic strains, thus requiring the measurement of very small strains [8], so that electrochemical effects have been investigated through the mechanical loading they induce on microcantilevers. An investigation of the double-layer region [10–13] (*i.e.*, when no electrochemical reaction occurred) as well as

adsorption reactions [14–17] and electrodeposition [18] have been carried out using the standard optical lever technique [1].

In order to further describe electrochemical phenomena at solid electrodes, several interferometric techniques have been used to provide descriptions of the electrochemically driven topographic or chemical changes occurring in the layer adjacent to an electrode [19–21]. In the special case of microcantilever inspection, it has been proven that using full-field interferometric measurements [22] to investigate the electro-elastic coupling provides redundant enough experimental information to build a model of the coupled interfacial phenomena [23]. Using such a spatially resolved information is then necessary, since a micro-cantilever is expected to behave as an “antenna”, thus yielding a charge localization near geometric singularities.

It is therefore proposed to adapt such a tool to describe at the local level as well as at the cantilever scale the way the electro-elastic coupling is altered by molecular adsorption. As the mechanical reaction to an electrochemical stimulus is found to be highly adsorption rate dependent, one considers the concept of electrochemically-actuated micromechanical sensors as a potential candidate for various real-life target molecules recognition problems. After a description of the experimental set-up and procedures, the adsorption process is described from the electrochemical and mechanical point of view. A dedicated framework is then proposed to analyze phase maps acquired when the cantilever undergoes an electrochemical actuation at different adsorption rates. This analysis shows that both the coupling intensity and the charge distribution are significantly altered by adsorption, so that using a device as simple as a cantilever is not optimal to provide a reliable detection scheme when the global mechanical response of the sensor is monitored.

2 Experimental procedure

2.1 *Experimental set-up*

A home-made fluid-cell is used to host an array of gold coated microcantilevers. This sample is fastened to a copper substrate with a conducting epoxy glue. The temperature of this copper substrate is controlled through Peltier effect modules and a temperature sensor. Another copper part, whose temperature is also controlled through Peltier modules, encapsulates this fluid-cell, whose content is modified with a fluid inlet and outlet.

The objects under consideration are micro-cantilevers ($70 \times 20 \times 0.84 \mu\text{m}^3$) that are made of 770-nm thick silica obtained by thermal oxidation of a silicon wafer. Titanium (20-nm thick) and 50-nm thick gold layers are then deposited onto the sample. The gold layer on top of the cantilevers is utilized as a working electrode in a KCl solution. All the connections are insulated with a thin PDMS layer to ensure that only the gold surface of the working electrode is in contact with the solution. It has a total area of almost 1 cm^2 in constant contact with the electrolytic solution.

2.2 *Surface activation*

After bubbling nitrogen, the fluid cell is then filled with a KCl solution (10^{-2} M), prepared from milliQ water. The gold surface is then cleaned electrochemically by performing successive cyclic voltammograms between 0 and 0.8 V at a rate of 10 mV/s. Gold is then successively oxidized and reduced, until a stable voltammogram (*i.e.*, after a few cycles) is obtained, thus ensuring a clean and

reproducible metallic surface. The fluid cell is then purged and filled again with a 10^{-2} M KCl deoxygenated solution.

2.3 *Cyclic voltammetry*

The potential window was chosen so that the electrode processes are not perturbed by any substance or electrochemical transformation of the electrode material. For potentials less than -0.1 V vs. Ag/AgCl, oxygen reduction may occur while a peak, presumably related to Au oxidation, is observed for potentials greater than 0.5 V. During three potential cycles, an optical phase map [22] is recorded every 0.05-V step, thus providing a set of 61 phase maps, that is a $15 \times 111 \times 61$ phase measurements stack covering the cantilever through the three potential cycles. The choice of the potential scan rate (2 mV/s) ensures that the electrode equilibrium is established in times much shorter than the time interval between two snapshots (25 s). The phase map acquisition is carried out during almost 1 s. Therefore the potential of the electrode is considered constant during this observation. Such cyclic voltammetry cycles have been performed before (CV0), during (CV1) and after (CV2) decane-thiol adsorption.

2.4 *Displacement field measurement*

The cantilever bending is monitored using a phase-modulated Nomarski imaging shear-interferometer [22]. The interference pattern is obtained as the difference of two topographies of the surface, shifted by a Wollaston prism by a distance d . The Wollaston shear-direction is chosen to be parallel to the

cantilever axis, denoted by \mathbf{x} , so that the topographies involved in the interference pattern are views of the cantilever shifted along the direction of its larger dimension (Fig. 1). The distance d is chosen to be similar in magnitude with the cantilever length.

Monitoring the induced quasi-static cantilever bending, the recorded phase map changes ϕ_{mes} are purely mechanical as long as there is no heterogeneous chemical surface modification [22], and is thus described solely by ϕ_{mec} , which arise from both surface out-of-plane displacement and rotation

$$\begin{aligned} \phi_{mec}(x, y) = & \frac{4\pi n_l}{\iota\lambda} (v(x, y) - v(x - d, y)) \\ & + \frac{\partial\phi_W}{\partial\gamma} \left(\frac{dv}{dx}(x, y) - \frac{dv}{dx}(x - d, y) \right) \end{aligned} \quad (1)$$

$v(x, y)$ is the out-of-plane displacement field and $\frac{\partial\phi_W}{\partial\gamma}$ is an experimentally identified coefficient, n_l the average refractive index of the ambient medium, λ the used wavelength, and ι a scaling coefficient depending on the numerical aperture of the objective lens. Section 3.3 deals with the case where heterogeneous surface reaction is expected. Throughout the reported experiments, the displacement field was observed to be homogeneous across the cantilever width, so that it is expanded onto a user-defined functions basis of the longitudinal coordinate x

$$v(x, n) = \sum_{r=1}^R \zeta_r(n) f_r(x) \quad (2)$$

where $\{\zeta_r(n)\}$ for $r \in \{1 \dots R\}$ is the projection of the displacement field v onto the basis $\{f_r(x)\}$ for the time step n . The displacement is then obtained from the measured phase stack by minimizing

$$\eta^2 = \frac{1}{N_p} \sum_{x,y,n} \chi(x, y, n)^2 \quad (3)$$

$$= \frac{1}{N_p} \sum_{x,y,n} \frac{1}{\mu(x, y, n)^2} (\phi_{test}(x, y, n) - \phi_{test}(x, y, n - 1) - \phi_{mes}(x, y, n) + \phi_{mes}(x, y, n - 1))^2 \quad (4)$$

where $\phi_{mes}(x, y, n) - \phi_{mes}(x, y, n - 1)$ is the measured phase change between two consecutive loading steps, $\phi_{test}(x, y, n) - \phi_{test}(x, y, n - 1)$ the phase change estimated from the test parameters ζ_r , N_p the number of measurement points and $\mu(x, y, n)^2$ the estimated phase change variance at the considered point. The optimal parameters set then provides the cantilever displacement field.

2.5 Decane-thiol adsorption

Decane-thiol from Sigma-Aldrich was diluted in ethanol to get a 7 mM decane-thiol solution. The latter was then diluted (1 % in volume) in the supporting electrolyte, namely 10^{-2} M KCl, before injection in the above-described fluid-cell. The refractive index change induced when mixing the decane-thiol solution with 10^{-2} M KCl is then negligible and does not perturb the imaging properties of the microscope. The cantilever quasi-static bending is then monitored (step 1: 1 image every 2 minutes during 5 hours; step 2: 1 image each 3 minutes during 7h30). In order to monitor the adsorption process, AC voltammetry scans have been carried before (DC0), during (DC1) and after (DC2) the decane-thiol adsorption. The electrode impedance was measured between -0.1 and 0.4 V vs. Ag/AgCl, at 20 Hz with a modulation amplitude of 25 mV. These AC voltammetry scans are performed prior to the three above-described voltammetry cycles. The experiment took place following the sequence DC0, CV0, adsorption step 1, DC1, CV1, adsorption step 2, DC2,

CV2, so that the consequence of decane-thiol adsorption on the electro-elastic coupling is assessed (Fig. 2).

3 Results and discussion

3.1 Electrochemical response of the microcantilevers array

Figure 3 shows the change of the measured overall capacitance during the adsorption process. The capacitance value decreases by a factor of 2 between the experiment start (DC0) and the first stop (DC1). The capacitance then does not evolve as fast, reaching a minimum value at the end of the adsorption process, thereby proving the electrode passivation (DC2). The potential of zero charge is obtained from the minimum of the differential capacity (DC0), and is about -0.05 V vs. Ag/AgCl, in agreement with values already reported for Au(111)/KCl 10^{-2} M systems [24]. In addition, the coverage ratio may be roughly estimated from the minimum capacitance values, assuming that the coverage ratio is 0 for DC0, and 1 at the end of the experiment (DC2). Considering that the electrode behavior is described by a capacitor [25,26] (representing the clean part of the electrode) in a branch parallel to a serial capacitors assembly [27] (representing the covered part of the electrode), the coverage ratio is estimated to be 0.71 for DC1, and the decane-thiol layer capacitance is estimated to be about $0.8 \mu\text{F}/\text{cm}^2$, in agreement with reported values [28]. The current flowing through the electrode is recorded during cyclic voltammetry scans.

3.2 Adsorption-induced cantilever bending

The adsorption process (*i.e.*, moving the molecules closer to the surface and considering their interaction) is highly favorable from a thermodynamics point of view, so that the interfacial system provides relatively large surface strains to reach mechanical equilibrium. This corresponds to the minimum overall enthalpy, leading to a decreased chemical enthalpy (because of decane-thiol adsorption process) and an increased elastic energy (because of cantilever bending) [29]. Adsorption is assumed to occur uniformly along the cantilever, so that it does not induce any additional phase contribution. The procedure detailed in Section 2.4 then holds. The identified quasi-static displacement fields along the median line of the cantilever using a polynomial basis $f_r(x) = x^r$ for r ranging from 1 to $R = 3$ are shown as functions of time in Fig. 4 for both adsorption steps. The minimum value of $\sqrt{\eta_{min}^2}$ is found to be around 10^{-10} for both adsorption steps, thereby proving that the displacement field is well described by a cubic polynomial. As already reported [30,31], upon adsorption of thiol the cantilever experiences a downward bending, suggesting that this adsorption is accompanied by a gold surface expansion. The maximum displacement is about 80 nm after 5 h (end of step 1) and 160 nm after step 2 (the initial states correspond to the beginning of adsorption steps 1 and 2, respectively). Let us underline the different time scales the displacement follows for the two adsorption steps:

- on the one hand, adsorption on a clean surface (step 1) yields a unique characteristic time scale;
- on the other hand, adsorption on a pre-adsorbed surface (step 2) exhibits a mechanical effect following two very different time scales, namely, a first

mechanical contribution takes place during a few minutes, whereas the full mechanical effect develops during several hours.

According to the literature, the formation kinetics of alkane-thiol self-assembled monolayer were investigated using various physico-chemical techniques including electrochemical [26], AFM [32], surface plasmon resonance (SPR) [33] and ellipsometry [34,35]. Even though there are some contradictions concerning the rate of formation of the layer, most of the studies deal with a two-stage adsorption process in agreement with what is observed herein. In principle, the present results may be compared with the two time scales identified by ellipsometric monitoring of adsorption process [35], even though it has been reported that the mechanical effect and the optical thickness of the adsorbed layer growth kinetics are not simply related [36]. For this reason and also because the adsorption process homogeneity along the micro-cantilever is difficult to assess, a deeper description of the kinetics of formation of the monolayer lies beyond the scope of the present paper. It is worth noting that this long-term monitoring of the mechanical effect induced by adsorption is achieved using differential interferometric measurements and all possible precautions to avoid any significant drift, which are not easily implemented in real-life applications.

3.3 Electrochemically-induced cantilever bending

In order to bypass the difficulty of performing long time measurements, which are likely to be subjected to significant drifts (*e.g.*, thermal), the displacement of the cantilever is modulated at a user-defined frequency. This is achieved by using the electro-elastic coupling that is stimulating electrochemically, during a cyclic voltammetry experiment, the deformation of the cantilever (Subsec-

tion 2.3). In that case, the measured phase map arises from both mechanical deformation of the cantilever and change in the interface composition owing to changes in the chemical composition of the double layer adjacent to the electrode, so that the procedure presented in Section 2.4 has to be modified. Because of the presence of a (partially) adsorbed layer, the method proposed in Ref. [23] has to be enriched. The thin electrolyte layer close to the surface, whose thickness scales as the Debye length λ_D , is significantly modified when charging the electrode. The concentration shift induced in this layer modifies locally the refractive index of the solution. In addition, charging the interface modifies the free electrons density in the metal, thus changing the complex refractive index of the metal [37]. Both contributions (as well as decane-thiol adsorption) modify the complex reflection coefficient of the interface, and therefore generate a non-mechanically induced optical phase change

$$\phi_{mes} = \phi_{mec} + \phi_{ec} \quad (5)$$

The measured phase ϕ_{mes} results from the mechanical contribution ϕ_{mec} and an additional electrochemical term ϕ_{ec} that is obtained by assuming that reflection occurs at the interface between two homogeneous layers:

- on the metallic side, the thickness is arbitrarily chosen to be 1 nm [37], and the refractive index is obtained according to Drude's model;
- the thickness of the liquid phase layer is chosen to be equal to $2\lambda_D + \vartheta\lambda_{ads}$, where λ_{ads} is the adsorbed decane-thiol film thickness, and ϑ is a mixing ratio. The parameter ϑ is not a coverage ratio but describes how much the ions penetrate the decane-thiol adsorbed layer during the cyclic voltammetry. The case when $\vartheta = 0$ may thus result either from a clean electrode (*i.e.*, no adsorption) or from an impenetrable adsorbed layer. The composition of

this layer is determined to ensure the same surface excess than predicted by the Gouy-Chapman theory, and the refractive index of this homogeneous layer is obtained from the Lorentz-Lorenz formula [38]. This significant enrichment, compared with the modeling we proposed in Ref. [23], allows one to deal with partially covered surfaces.

For ions, the molar volumes and refractivities are taken from the literature [39,40], namely, $\lambda_{ads} = 1.5$ nm is obtained from published estimates [28], while the molar refractivity for the decane-thiol is obtained from Ref. [41]. The above assumptions allow one to compute the electrochemical contribution as a function of the surface charge density field and the mixing ratio, using Fresnel's equations for a given equivalent incidence angle θ_e and both TE and TM polarizations [42]

$$\phi_{ec}(x, y, \vartheta, \theta_e) = \phi_{TE, TM}(\sigma_m(x, y), \vartheta, \theta_e) - \phi_{TE, TM}(\sigma_m(x - d, y), \vartheta, \theta_e) \quad (6)$$

The influence of θ_e is found to be negligible when compared with ϑ . In previous investigations of the electro-elastic coupling on clean cantilevers [23] the microcantilever bending was observed to result from a non-uniform mechanical loading. It was interpreted as a singular charging of the microcantilever edge in agreement with non-uniform current distribution at microelectrodes [43,44]. The integration of the current with respect to time then provides the overall charge carried by the working electrode Q as a function of the potential. A good correlation between the mechanical behavior of the cantilever and the surface electrochemical response was obtained when considering that the local charge density σ_m at a distance x from the field border on the substrate is

distributed according to

$$\sigma_m(x, Q) = D(x) \times Q \quad (7)$$

where Q is the overall surface charge of the entire electrode, and the localization function is written as

$$D(x) = \frac{c_q(x_0)}{(x_0 - x)^p} \quad (8)$$

where the constant $c_q(x_0)$ is defined so that $D(x) = 1$ when x tends to the field border on the substrate, x_0 and p are used to describe the position and order of the singular charge density field, respectively. A similar framework is used herein.

In addition, the mechanical contribution is obtained by assuming that the cantilever is subjected to a shear-stress field $\tau(x)$, which is a continuous function of the local charge density σ_m . This local relationship is then expanded onto a polynomial basis

$$\tau(x) = \sum_{t=1}^T \delta_t \sigma_m^t(x) \quad (9)$$

where $\{\delta_t\}$ are the coefficients describing the local coupling relationship to be found. For a given charge density field, the displacement field induced by each component of Eq. (9) is derived by using the Euler-Bernoulli beam theory [45], thus yielding the functions basis $f_t(x)$ defined in Eq.2. To summarize, each cross-section is assumed to remain planar during deformation, so that the local beam curvature is obtained from the bending moment M_b generated by the

shear-stress τ applied to the cantilever

$$M_b = EI \frac{d^2 v(x)}{dx^2} = - \int_x^L b e \tau(\xi) d\xi \quad (10)$$

where b denotes the cantilever width, EI its flexural stiffness, and e the distance from the neutral axis to the gold surface. Setting arbitrarily the equivalent incidence angle to $\theta_e = 0.3$ rad (this does not significantly affect the following results), one is then able to compute a trial phase field, and thus to find the optimal set of parameters $\{p, x_0, \vartheta, \delta_t\}$ describing the electro-elastic test under scrutiny by minimizing the function defined by Eq. (3). Linearizing this latter function with respect to its parameters close to the solution, an estimate for the standard deviation of the identified parameters is obtained from the measurement reproducibility.

Table 1 shows the identified parameters for the three electro-elastic tests, namely, CV0, CV1 and CV2. For all the considered tests, $T = 3$ is found to provide the best compromise between the coupling description and the minimization robustness. Changing the arbitrarily chosen θ_e value has no significant effect on the following results. The residual η_{min}^2 is small compared to 1, meaning that the phase change fields all over the 3 potential cycles are well described by the proposed modeling. In addition, an upper bound Γ_ϑ for the standard deviation on ϑ resulting from the measurement uncertainties is provided to assess its identifiability.

Figure 5 shows the identified displacement field along the cantilever as a function of the loading step during the potential cycles for CV0 and CV2. Contrary to decane-thiol adsorption, the cantilever subjected to the electro-elastic coupling experiences an upward bending, as already reported [10,11,23]. The

displacement amplitude is significantly decreased when moving from the clean electrode (CV0: above 100 nm maximum displacement) to the blocked electrode (CV2: 45 nm maximum displacement). In addition, the displacement field and its change during the test are altered, and a mechanical description of the measured effect is obtained through the identification procedure.

The identified localization functions $D(x)$, describing the surface charge singularity on the cantilever edge and modeled by the p and x_0 parameters, are plotted in Fig. 6. Similarly to the clean electrode case [23], the surface charge density is highly localized close to the cantilever edge, thereby proving that one should use local shear-stress fields instead of a global “surface stress” concept to describe mechanical effects at the micro-cantilever scale. Similarly, it is preferable to deal with charge densities measured at the level of a single cantilever instead of the global charge density measured on a large electrode. This is not possible with the current experimental set-up, it is currently attempted to improve this issue. Alkane-thiol adsorption induces a significant change in the surface charge distribution, namely, even though the overall electrode charge range decreases when moving to blocked surfaces, the charge distribution tends to be more and more uniform. One should underline that this tendency is not satisfied for CV1, where the “antenna” effect seems to be first enhanced by the adsorption process, probably because of an easier electrode blockage far from the edges.

The significant change in the electrochemical behavior of the electrode is also obtained in Fig. 7, where the identified electro-elastic coupling relationships (defined in Eq. (9) and the identified δ_t coefficients reported in Table 1) are shown in their identification range, that is in the identified charge density range. The decrease in the overall charge together with the decrease in sin-

gularity of the localization function yield a dramatically reduced local charge density range for fully adsorbed state (CV2) compared to the early steps (CV0 and CV1). It is also worth noting that the deformation accumulation observed for CV2 is well described by the charge accumulation on the electrode.

The identified ϑ value for CV0 is close to zero, which is consistent with the fact that the electrode is initially free of thiols. The residual is not significantly affected by enforcing $\vartheta = 0$ during minimization. On the other hand, the identified mixing parameter ϑ remains fairly low for the intermediate step, even though the electrode is partially covered (Subsection 3.1), thereby proving that the ions do not penetrate the added layer, which is thus hydrophobic. This is known as a characteristic feature of alkane-thiol films [46]. Again, the identification results are not significantly modified by setting $\vartheta = 0$. For the last step (CV2), because the charge density field becomes uniform, the optical properties of the surface no longer influence the measured (*i.e.*, differential) phase field, so that the mixing parameter is no longer identifiable with the proposed technique, as shown by the large value obtained for Γ_{ϑ} (the ϑ value is therefore not displayed in Table 1). There is therefore room for experimental improvements.

If the coupling relationship is not significantly modified by the first adsorption step (*i.e.*, the identified relationship for CV0 lies within the confidence range around the identified relationship for CV1), the increase in the initial slope of the coupling relationship is significant after the second adsorption step, thereby providing an information complementary to the quasi-static bending of the cantilever (Fig. 7). Qualitatively, the alkane-thiol film increases the closest approach distance of ions from the electrode, thereby decreasing the charge carried by the electrode at a given potential. On the other hand, the

dielectric constant of the surface is increased by the adsorption process, so that the electrostatic free energy of the surface is significantly higher, for a given charge density, when adsorption occurs. The stored electrochemical energy is then higher for a given surface charge density, so that the electro-elastic coupling (at a given charge) is enhanced [29]. The quantitative evaluation of the electro-elastic coupling modification as a function of the adsorbed layer would require a more detailed characterization of the interface [17].

Using full-field measurements to investigate the effects of decane-thiol adsorption, it is shown that the significant decrease in the maximum shear-stress (by a factor of 10 as seen from Fig. 7) is partially compensated by the surface charge redistribution induced by adsorption, thus resulting in a limited cantilever tip displacement ratio before and after adsorption (almost equal to 2 as seen from Fig. 5). It is therefore necessary to take into account these global and local effects when designing electrochemically-actuated sensors in order to save their tremendous potential compared with the long-term, drift sensitive, and purely mechanical measurements developed for micro-cantilever sensors.

4 Conclusion

A metal coated micro-cantilever was utilized simultaneously as a micro-electrode and a micromechanical sensor. Electrochemical and full-field interferometric measurements were carried out to monitor both surface composition changes and cantilever displacements during cyclic voltammetry, before, during and after decane-thiol adsorption. The use of full-field measurements and a dedicated identification technique allows one to monitor the effects of decane-thiol adsorption on the electro-elastic coupling, namely, the charge density quasi-

singularity on the cantilever edge vanishes, and the electro-elastic coupling relationship is significantly modified. This result shows that the mechanisms involved in the adsorption-induced electro-elastic coupling alteration on a microcantilever need to be described at the local as well as at the cantilever scale, thus revealing the local and global nature of the alteration. The results reported herein show that even though the local passivation decreases by a factor 10 the maximum stress acting on the cantilever, the tip displacement is reduced by only a factor 2 because of the simultaneous charge redistribution. These effects should therefore be considered when designing optimized electro-chemically actuated sensors in order to make the most of their potential.

References

- [1] N.V. Lavrik, M.J. Sepaniak and P.G. Datskos, Cantilever transducers as a platform for chemical and biological sensors, *Rev. Sci. Instrum.* *75* (2004) 2229-2253.
- [2] B. Ilic, D. Czaplewski, H.G. Craighead, P. Neuzil, C. Campagnolo and C. Batt, Mechanical resonant immunospecific biological detector *Appl. Phys. Lett.* *77* (2000) 450-452.
- [3] N.V. Lavrik and P.G. Datskos, Femtogram mass detection using photothermally actuated nanomechanical resonators *Appl. Phys. Lett.* *82* (2003) 2697-2699.
- [4] B. Ilic, H.G. Craighead, S. Krylov, W. Senaratne, C. Ober and P. Neuzil, Attogram detection using nanoelectromechanical oscillators *J. Appl. Phys.* *95* (2004) 3694-3703.
- [5] A. Gupta, D. Akin and R. Bashir, Single virus particle mass detection using microresonators with nanoscale thickness *Appl. Phys. Lett.* *84* (2004) 1976-1978.
- [6] J. Fritz, M.K. Baller, H.P. Lang, H. Rothuizen, P. Vettiger, E. Meyer, H. Güntherodt, C. Gerber and J.K. Gimzewski, Translating biomolecular recognition into nanomechanics *Science* *288* (2000) 316-318.
- [7] L.A. Pinnaduwaage, V. Boiadjev, J.E. Hawk and T. Thundat, Sensitive detection of plastic explosives with self-assembled monolayer-coated microcantilevers *Appl. Phys. Lett.* *83* (2003) 1471-1473.
- [8] V.A. Marichev, Partial charge transfer during anion adsorption Methodological aspects *Surf. Sci. Rep.* *56* (2005) 277-324.
- [9] L. Jaeckel, G. Lang and K.E. Heusler, New interferometric method to investigate surface energies at solid electrodes *Electrochim. Acta* *39* (1994) 1031-1038.

- [10] R.A. Fredlein and J.O.M. Bockris, An electrocapillary study of the gold-perchloric acid solution interface *Surf. Sci.* *46* (1974) 641-652.
- [11] R. Raiteri and H.J. Butt, Measuring electrochemically induced surface stress with an atomic force microscope *J. Phys. Chem.* *99* (1995) 15728-15732.
- [12] F. Tian, J.H. Pei, D.L. Hedden, G.M. Brown and T. Thundat, Observation of the surface stress induced in microcantilevers by electrochemical redox processes *Ultramicroscopy* *100* (2005) 217-223. See also the comment by G.G. Láng, T.A. Rokob and G. Horányi, *Ultramicroscopy* *104* (2005) **104**, 330-332.
- [13] D. Lee, T. Thundat and S. Jeon, Electromechanical identification of molecules adsorbed on microcantilevers *Sensors and Actuators B* *124* (2007) 143-146.
- [14] V. Tabard-Cossa, M. Godin, L. Y. Beaulieu and P. Grütter, A differential microcantilever-based system for measuring surface stress changes induced by electrochemical reactions *Sens. Act. B* *107* (2005) 233-241.
- [15] H. Ibach, C.E. Bach, M. Giesen and A. Grossman, Potential-induced stress in the solid-liquid interface: Au(111) and Au(100) in an HClO₄ electrolyte *Surf. Sci.* *375* (1997) 107-119.
- [16] W. Haiss, Surface stress of clean and adsorbate-covered solids *Rep. Prog. Phys.* *64* (2001) 591-648.
- [17] V. Tabard-Cossa, M. Godin, I.J. Burgess, T. Monga, R.B. Lennox and P. Grütter, Microcantilever-based sensors: effect of morphology, adhesion, and cleanliness of the sensing surface on surface stress *Anal. Chem.* *79* (2007) 8136-8143.
- [18] T.A. Brunt, T. Rayment, S.J. O'Shea and M.E. Welland, Measuring the surface stresses in an electrochemically deposited metal monolayer: Pb on Au (111) *Langmuir* *12* (1996) 5942-5946.

- [19] H.S. White, D.J. Earl, J.D. Norton and H.J. Kragt, In situ topographical imaging of electrode surfaces using high-resolution phase measurement interferometric microscopy *Anal. Chem.* *62* (1990) 1130-1134.
- [20] C.P. Smith, H.L. Kennedy, H.J. Kragt, H.S. White and J.F. Biegen, Phase-measurement interferometric microscopy of microlithographically fabricated platinum electrodes *Anal. Chem.* *62* (1990) 1135-1138.
- [21] Q. Li and H.S. White, Interferometric measurement of a depletion layer structure and volumetric data in concentrated organic redox solutions *Anal. Chem.* *67* (1995) 561-569.
- [22] F. Amiot and J.P. Roger, Nomarski imaging interferometry to measure the displacement field of micro-electro-mechanical systems *Appl. Optics* *45* (2006) 7800-7810.
- [23] F. Amiot, F. Hild, F. Kanoufi and J.P. Roger, Identification of the electroelastic coupling from multi-physical fields measured at the micrometre scale *J. Phys. D: Appl. Phys.* *40* (2007) 3314-3325.
- [24] J. Clavilier and N. Van Huong, Etude de la structure de la couche double sur les electrodes d'or *J. Electroanal. Chem.* *41* (1973) 193-199.
- [25] B.B. Damaskin, O.A. Petrii, and V.V. Batrakov, in *Adsorption of Organic Compounds on Electrodes*, Plenum Press, New York, 1971.
- [26] R. Subramanian and V. Lakshminarayanan, Study of kinetics of adsorption of alkanethiols on gold using electrochemical impedance spectroscopy *Electrochim. Acta* *45* (2000) 4501-4509.
- [27] A.M. Becka and C.J. Miller, Electrochemistry at ω -hydroxy thiol coated electrodes. 4. Comparison of the double-layer at ω -hydroxy thiol and alkanethiol monolayer coated Au electrodes *J. Phys. Chem.* *97* (1993) 6233-6239.

- [28] M.D. Porter, T.B. Bright, D.L. Allara and C.E.D. Chidsey, Spontaneously organized molecular assemblies. 4. Structural characterization of n-alkyl thiol monolayers on gold by optical ellipsometry, infrared spectroscopy, and electrochemistry *J. Am. Chem. Soc.* *109* (1987) 3559-3568.
- [29] F. Amiot, A model for chemically-induced mechanical loading on MEMS *JoMMS (2) 9* (2007) 1787-1803.
- [30] R. Berger, E. Delamarche, H.P. Lang, C. Gerber, J.K. Gimzewski, E. Meyer and H. Güntherodt, Surface stress in the self-assembly of alkanethiols on gold probed by a force microscopy technique *Appl. Phys. A.* *66* (1998) S55-S59.
- [31] R. Berger, E. Delamarche, H.-P. Lang, C. Gerber, J.K. Gimzewski, E. Meyer and H.-J. Güntherodt Surface stress in the self-assembly of alkanethiols on gold *Science* *276* (1997) 2021-2024.
- [32] K. Hu and A.J. Bard, In situ monitoring of kinetics of charged thiol adsorption on gold using an atomic force microscope *Langmuir* *14* (1998) 4790-4794.
- [33] R.F. DeBono, G.D. Loucks, D.D. Manna and U.J. Krull, Self-assembly of short and long-chain n-alkyl thiols onto gold surfaces: A real-time study using surface plasmon resonance techniques *Can. J. Chem.* *74* (1996) 677-688.
- [34] C.D. Bain, E.B. Troughton, Y.-T. Tao, J. Evall, G.M. Whitesides and R.G. Nuzzo, Formation of monolayer films by the spontaneous assembly of organic thiols from solution onto gold *J. Am. Chem. Soc.* *111* (1989) 321-335.
- [35] F.S. Damos, R.C.S. Luz and L.T. Kubota, Determination of thickness, dielectric constant of thiol films, and kinetics of adsorption using surface plasmon resonance *Langmuir* *21* (2005) 602-609.
- [36] M. Godin, O. Laroche, V. Tabard-Cossa, L.Y. Beaulieu, P. Grütter and P.J. Williams, Combined in-situ micromechanical cantilever-based sensing and ellipsometry *Rev. Sci. Instrum.* *74* (2003) 4902-4907.

- [37] W.-P. Paik, M.A. Genshaw and J.O.M. Bockris, The adsorption of anions at the solid-solution interface *J. Phys. Chem.* *74* (1970) 4266-4275.
- [38] M. Stedman, Reflectance and ellipsometry of Metal/Electrolyte Interfaces *Trans. Faraday Soc.* (1970) 64-71.
- [39] T.C. Waddington, Ionic radii and the method of the undetermined parameter *Trans. Faraday Soc.* *62* (1966) 1482.
- [40] R. Zana and E. Yeager, Ultrasonic vibration potentials and their use in the determination of ionic partial molal volumes *J. Phys. Chem.* *71* (1967) 521-536.
- [41] E.J. Kupchik, General treatment of the heteroatoms with the randic molecular connectivity index *Quant. Struct.-Act. Relat.* *8* (1989) 98-103.
- [42] M. Born and E. Wolf, in *Principles of optics*, 6th edition, Pergamon Press, 1980.
- [43] R.G. Maus, E.M. McDonald and R.M. Wightman, Imaging of nonuniform current density at microelectrodes by electrogenerated chemiluminescence *Anal. Chem.* *71* (1999) 4944-4950.
- [44] C. Combellas, S. Nunige, and F. Kanoufi, Surface modification of halogenated polymers. 10. Redox catalysis induction of the polymerization of vinylic monomers. Application to the localized graft copolymerization of poly(tetrafluoroethylene) surfaces by vinylic monomers *Chem. Mater.* *19* (2007) 3830-3839.
- [45] S.P. Timoshenko and J.N. Goodier in *Theory of Elasticity*, 3rd edition, McGraw-Hill, New York (USA), 1970.
- [46] Finklea, H.O.; in *Electroanalytical chemistry*, A.J. Bard and I Rubinstein (Eds.) Marcel Dekker Inc (New York), 1996.

List of Tables

- 1 Identified parameters for the different cyclic voltammetry experiments, describing the surface charge density, the interface composition, the coupling relationship and the identification quality. The coupling relationship coefficients are normalized with respect to the cantilever flexural stiffness:

$$\tilde{\delta}_i = \frac{be\delta_i}{EI} \quad 26$$

Table 1

Identified parameters for the different cyclic voltammetry experiments, describing the surface charge density, the interface composition, the coupling relationship and the identification quality. The coupling relationship coefficients are normalized with respect to the cantilever flexural stiffness: $\tilde{\delta}_i = \frac{be\delta_i}{EI}$

CV test	CV0	CV0	CV1	CV1	CV2
p	2.28	2.51	3.55	3.68	4.47
$\frac{x_0}{L}$	1.08	1.07	1.20	1.14	2.11
ϑ (unitless)	7×10^{-2} identified	0 prescribed	9×10^{-2} identified	0 prescribed	#
Γ_ϑ	0.32		0.19		10^7
$\tilde{\delta}_1$ (C^{-1})	-3.13×10^3	-3.18×10^3	-5.25×10^3	-5.76×10^3	-2.18×10^5
$\tilde{\delta}_2$ ($m^2.C^{-2}$)	-2.04×10^2	-2.05×10^2	-1.18×10^2	-1.31×10^2	1.66×10^5
$\tilde{\delta}_3$ ($m^4.C^{-3}$)	1.07×10^{-1}	1.09×10^{-1}	8.40×10^{-2}	9.40×10^{-2}	-1.48×10^5
residual η_{min}^2	6.3×10^{-2}	6.3×10^{-2}	5.8×10^{-2}	5.8×10^{-2}	8.5×10^{-2}

List of Figures

- 1 Schematic view of the imaging set-up and typical interference pattern. The shear direction is parallel to the cantilever direction, and the shear distance d is almost equal to the cantilever length. The axis system is shifted for the sake of clarity and the origin is set at point O. 29
- 2 Schematic view of the system considered to assess the effect of decane-thiol adsorption on the electro-elastic coupling at both the local and cantilever scales. 30
- 3 Measured differential capacity of the microcantilevers array in a 10^{-2} M KCl solution before (DC0), during (DC1) and after (DC2) decane-thiol adsorption; starting potential -0.1 V vs. Ag/AgCl. 31
- 4 Identified out-of-plane quasi-static displacement field along the median line of the cantilever as a function of adsorption time: a) step 1, b) step 2. 32
- 5 Identified out-of-plane displacement field along the median line of the cantilever during cyclic voltammetry cycles: a) CV0, b) CV2. 33
- 6 Identified localization functions $D(x)$ for the three electro-elastic tests before (CV0), during (CV1) and after (CV2) decane-thiol adsorption. 34

- 7 Identified electro-elastic coupling relationships before (CV0), during (CV1) and after (CV2) decane-thiol adsorption, with estimated confidence range from the standard deviation on the identified parameters for step CV1.

35

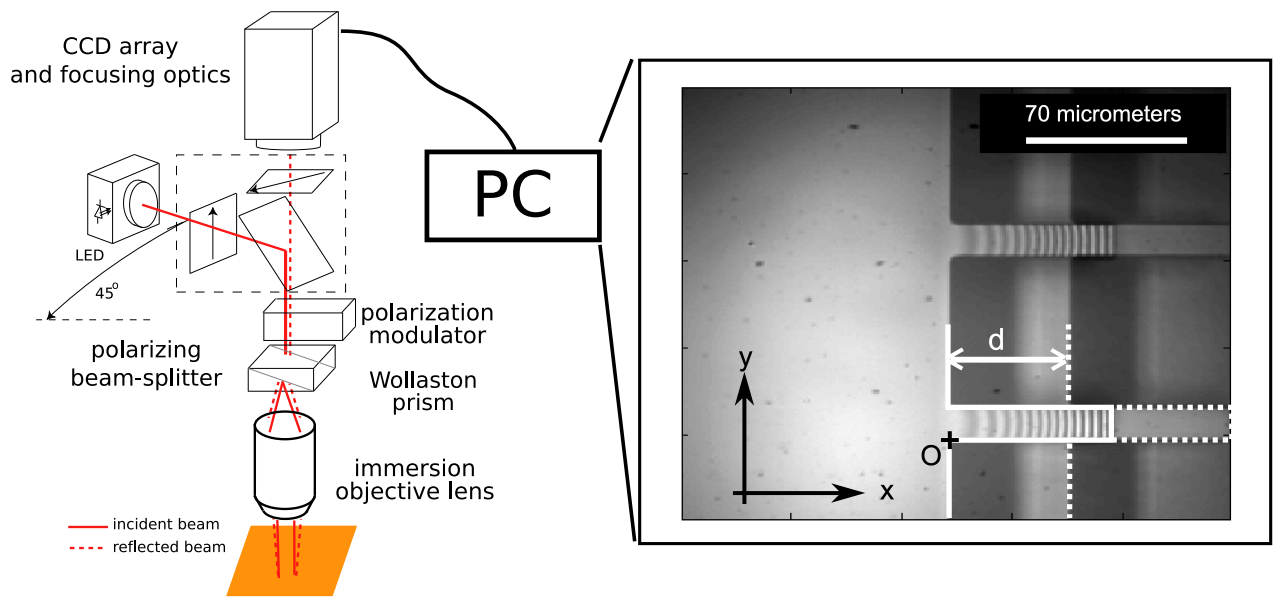


Fig. 1. Schematic view of the imaging set-up and typical interference pattern. The shear direction is parallel to the cantilever direction, and the shear distance d is almost equal to the cantilever length. The axis system is shifted for the sake of clarity and the origin is set at point O.

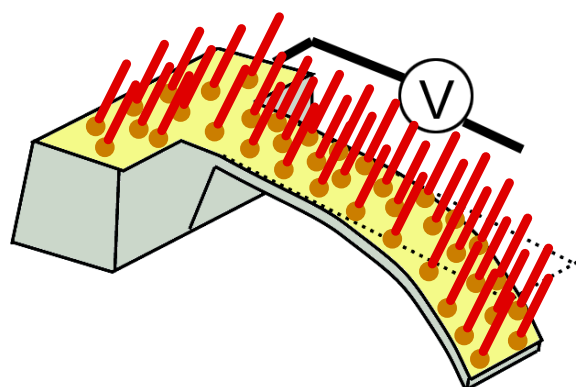


Fig. 2. Schematic view of the system considered to assess the effect of decane-thiol adsorption on the electro-elastic coupling at both the local and cantilever scales.

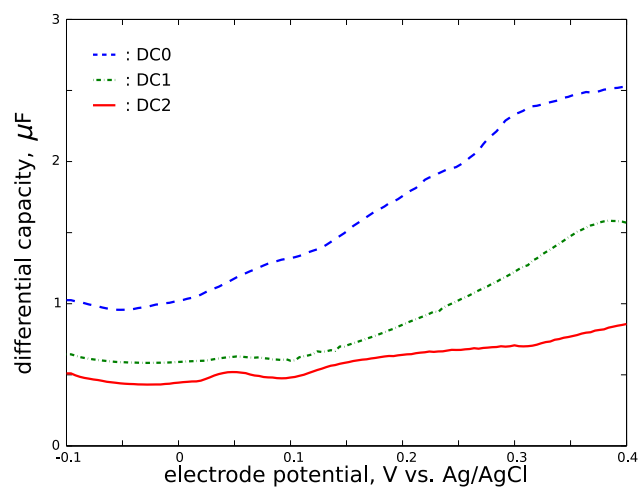


Fig. 3. Measured differential capacity of the microcantilevers array in a 10^{-2} M KCl solution before (DC0), during (DC1) and after (DC2) decane-thiol adsorption; starting potential -0.1 V vs. Ag/AgCl.

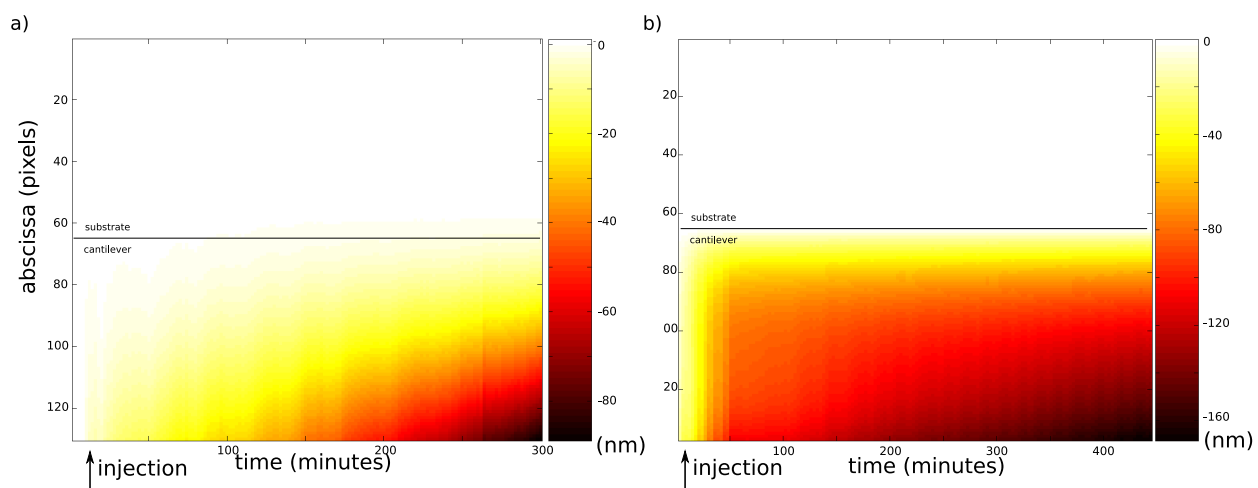


Fig. 4. Identified out-of-plane quasi-static displacement field along the median line of the cantilever as a function of adsorption time: a) step 1, b) step 2.

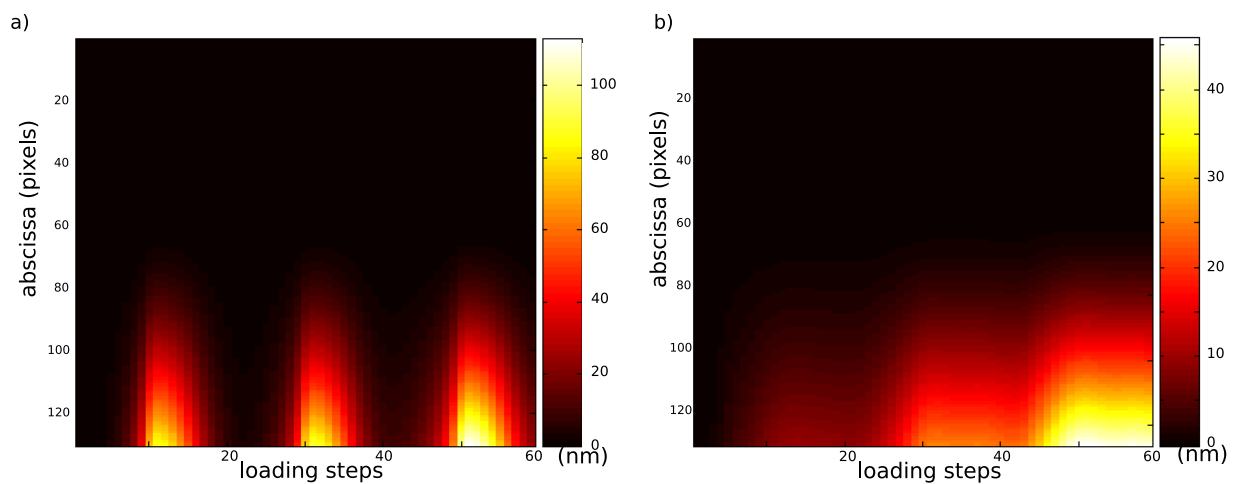


Fig. 5. Identified out-of-plane displacement field along the median line of the cantilever during cyclic voltammetry cycles: a) CV0, b) CV2.

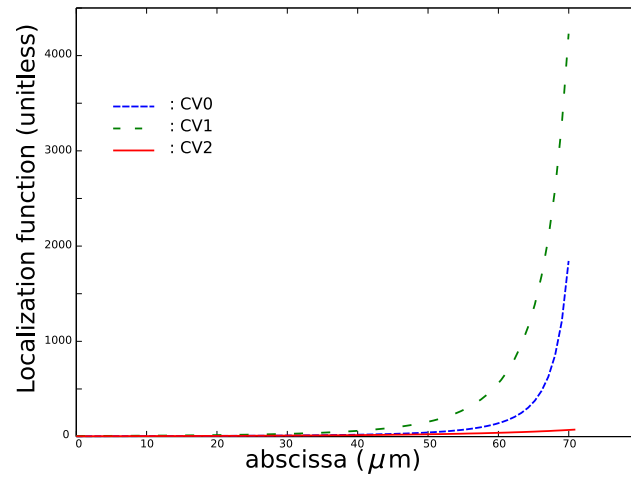


Fig. 6. Identified localization functions $D(x)$ for the three electro-elastic tests before (CV0), during (CV1) and after (CV2) decane-thiol adsorption.

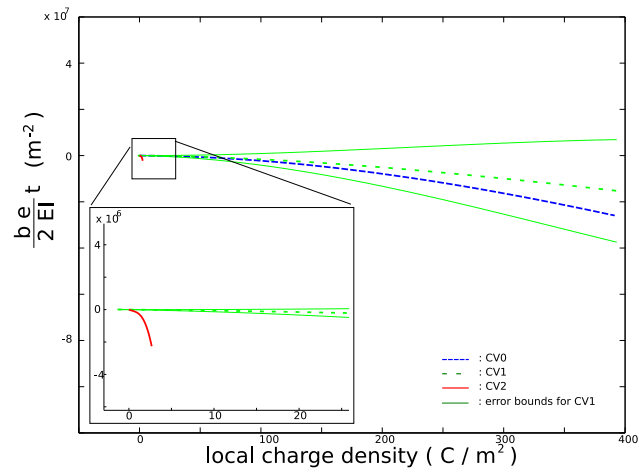


Fig. 7. Identified electro-elastic coupling relationships before (CV0), during (CV1) and after (CV2) decane-thiol adsorption, with estimated confidence range from the standard deviation on the identified parameters for step CV1.